Atmospheric Research 316 (2025) 107939

Contents lists available at ScienceDirect

Atmospheric Research

journal homepage: www.elsevier.com/locate/atmosres

Improving air pollution source apportionment in size-segregated PM using Pb isotope-based Bayesian mixing models in Tarragona (Spain)

Edson Plasencia Sánchez [a,*], Mònica Rosell [a], Clara Torrentó [a], Francisco Sánchez-Soberón [b,1], Joaquim Rovira [b,c], Jordi Sierra [b,d], Marta Schuhmacher [b], Albert Soler [a], David Widory [e]

[a] Grup MAiMA, Mineralogia Aplicada, Geoquímica i Hidrogeologia (MAGH), Departament de Mineralogia, Petrologia i Geologia Aplicada, Facultat de Ciències de la Terra, Institut de Recerca de l'Aigua (IdRA), Universitat de Barcelona (UB), Martí Franquès s/n, 08028 Barcelona, Spain
[b] Universitat Rovira i Virgili (URV), Environmental Analysis and Management Group, Departament d'Enginyeria Química, Av. Països Catalans 26, 43007 Tarragona, Catalonia, Spain
[c] Laboratory of Toxicology and Environmental Health, School of Medicine, IISPV, University Rovira and Virgili, Sant Llorenç 21, Catalonia, Reus 43201, Spain
[d] Laboratory of Soil Science, Faculty of Pharmacy and Food Sciences, Universitat de Barcelona (UB), Av. Joan XXIII s/n, 08028 Barcelona, Catalonia, Spain
[e] GEOTOP, Université du Québec à Montréal, Canada

ARTICLE INFO

Keywords:
PM10
PM2.5
PM1
Mixing Models
Lead isotope ratios
Inhalation exposure
Non-carcinogenic risk
Tarragona

ABSTRACT

A total of 75 outdoor PM_{10}, $PM_{2.5}$, and PM_1 samples from 14 schools, and 9 samples from potential local emission sources, were collected and analysed for their metallic content and lead (Pb) isotope ratios in 2 seasonal campaigns in Tarragona (Catalonia, Spain) to identify and apportion contamination sources and to assess associated health risks. Lead was predominantly found in PM_1, and although its levels were below air quality standards, its Enrichment Factors (EF), along with those of other potentially toxic elements (Cd, Cr, Cu and Sb), indicated extremely severe enrichment in all PM sizes. Seasonal differentiation in Pb enrichment was particularly significant in PM_1 during the cold campaign. This suggests an anthropogenic origin, mainly from combustion processes such as road traffic and a municipal solid waste incinerator, as supported by profiles of other metals (Cu, V and Zn) and the spatial distribution of the EF_{Pb}, respectively. Non-radiogenic Pb isotope ratios ($^{208}Pb/^{204}Pb$ and $^{206}Pb/^{204}Pb$) indicated a geogenic origin in some PM_{10} samples, based on their similarity to the geochronology of specific Spanish ore samples. However, radiogenic ratios ($^{208}Pb/^{207}Pb$ and $^{206}Pb/^{207}Pb$) pointed to coal-fired electrical plants (EGUs) and road traffic as the sources of the majority of the samples. These findings were corroborated by EF spatial distribution maps and by our previous study coupling air masses back trajectories with C and N isotopes in the same PM samples. Bayesian mixing models using both ^{204}Pb- and ^{207}Pb-normalised Pb isotope ratios estimated sources' contributions as follows: i) municipal solid waste incinerator (at least 10 % in PM_{10} and up to 60 % in both $PM_{2.5}$ and PM_1); ii) road traffic (up to 40 % for all size fractions); iii) coal-fired EGUs (around 20 % for all size fractions); and iv) geogenic particles (<10 % for all size fractions). Despite this strong contribution of anthropogenic sources, the potential health impacts of potentially toxic elements exposure were low, i.e., 3 additional cancer cases for adults per million of people due to Pb exposure, which nonetheless is comparable to levels observed in cities with populations 30 or more times larger than that of Tarragona.

1. Introduction

Airborne particulate matter (PM) has been classified as carcinogenic (Group 1) by the International Agency for Research on Cancer (IARC - International Agency for Research on Cancer, 2013), based on strong evidence that it harmfully affects human health (e.g. Loomis et al., 2013). Potentially toxic elements present in this PM have been proved to accumulate in human tissues via inhalation, to be able to reach the lung alveoli in their smallest fractions, and to cause both short- and long-term adverse health effects, especially for children (e.g. Kampa and Castanas, 2008). Among these metals, lead (Pb) is a neurotoxic element (e.g., Lanphear et al., 2003; Lanphear et al., 2005), ubiquitous in modern technologies and one of the most persistent anthropogenic pollutants (Settle and Patterson, 1980; Chang et al., 2016).

* Corresponding author.
E-mail address: eplasencia@ub.edu (E. Plasencia Sánchez).
[1] National Centre for Environmental Health, Instituto de Salud Carlos III, Ctra. Majadahonda-Pozuelo km 2.2, Majadahonda, Madrid 28220, Spain.

https://doi.org/10.1016/j.atmosres.2025.107939
Received 18 September 2024; Received in revised form 26 December 2024; Accepted 18 January 2025
Available online 21 January 2025

Identifying sources of Pb and other potentially toxic elements in PM is thus critical for mitigating risk to human health. Pb is directly released to the atmosphere from the mining and smelting of Pb-containing ores, through the combustion of Pb-containing fuels (e.g., coal and gasoline), or from the release of abrasion-generated road paint particles (Komárek et al., 2008). Relative concentration of chemical elements with respect to their Upper Continental Crust concentration, known as Enrichment Factors (EF), is a widely employed metric for elucidating the geogenic ($EF < 10$) or anthropogenic ($EF > 10$) origin of Pb and other potentially toxic elements in the environment (e.g. De la Cruz et al., 2009; Nory et al., 2021).

Lead isotope ratios (IRs) offer an alternative method for Pb sourcing in the environment, which, unlike the EF and other approaches, can be used as fingerprints of specific Pb sources (De la Cruz et al., 2009; Sun et al., 2014; Dai et al., 2023). Ore processing, smelting, and casting do not generate isotope fractionation (Ault et al., 1970; Kylander et al., 2010), and, thus, Pb IRs are directly linked to the origin of the raw material. Lead possesses four stable isotopes, ^{208}Pb, ^{206}Pb, ^{207}Pb and ^{204}Pb, whose abundances are ≈52 %, 24 %, 23 % and 1 %, respectively (CIAAW - Commission on Isotopic Abundances and Atomic Weights and International Union of Pure and Applied Chemestry, 2024). While ^{206}Pb, ^{207}Pb and ^{208}Pb represent the end-products of the ^{238}U, ^{235}U and ^{232}Th decay chains, respectively (Audi et al., 2003), ^{204}Pb is the only non-radiogenic isotope. Therefore, IRs for any Earth material are shaped by its initial U, Th and Pb concentrations, its age and the half-life of parent isotopes. The ores preserve the Pb crustal isotope ratio they acquired at the time of their formation (Dickin, 1995; Amelin and Neymark, 1998; Faure and Mensing, 2005). Therefore, the younger the geological ore, the more radiogenic its isotopic signature, i.e., higher $^{20X}Pb/^{204}Pb$ ratios (with X = 6, 7, or 8), along with higher $^{206}Pb/^{207}Pb$ and $^{208}Pb/^{207}Pb$ ratios. For example, very old ores, such as the Broken Hill ore (formed around 1.7 billion years ago and used in European leaded gasoline), are characterized by $^{206}Pb/^{207}Pb$ ratios ranging between 1.05 and 1.13, whereas younger ones (formed hundreds of millions of years ago during the Jurassic or Miocene eras) fall within 1.18 and 1.25 (Deboudt et al., 1999; Hansmann and Köppel, 2000). Therefore, anthropogenic Pb sources possess distinct isotopic ratios, reflective of the specific ore deposits they are derived from (Sangster et al., 2000).

Interpretation of Pb IRs is usually performed studying bivariate isotope plots that compare the characteristics of the study samples to those of known sources (Monna et al., 2000; Bird et al., 2010; Álvarez-Iglesias et al., 2012). While this approach is adequate for interpreting well determined systems, such as discriminating anthropogenic vs. lithogenic Pb or petrol-derived vs. ore-derived Pb sources, it has limitations in the presence of three or more mixing endmembers. In such cases, Bayesian mixing models have recently been successfully applied to solve Pb apportionment in complex anthropogenic environments (e.g., Longman et al., 2018; Anaman et al., 2024). Indeed, recent studies have applied these models for apportioning Pb sources in PM samples, focusing mainly on coarse particles (Dietrich et al., 2021; Wu and Huang, 2021; Ray et al., 2024), and barely on fine particles (Chen et al., 2023). To our knowledge, Pb isotope-based Bayesian models have not been applied yet for submicron particles.

With that in mind, the objective of this study was to use a Bayesian mixing model based on Pb IRs to identify and apportion atmospheric pollution sources in an urban and industrial complex city using size-segregated PM samples comprising 3 PM size fractions: PM_{10}, $PM_{2.5}$ and PM_1 (i.e., PM with aerodynamical diameters equal or inferior to 10, 2.5, and 1 μm, respectively), considering that smaller particles deeply reach lungs and therefore are more harmful. PM samples were previously collected from 14 schools in Tarragona (Spain) in 2 seasonal outdoor air sampling campaigns, as most people's activities are seasonal compared to industrial ones that remain somewhat constant through the year (Sánchez-Soberón et al., 2019; Plasencia Sánchez et al., 2023). In this study, we characterized them for Pb concentrations and used their Pb isotopic compositions in a Bayesian mixing model (MixSIAR model, Stock and Semmens, 2016) to qualitatively and quantitatively identify and apportion Pb pollution sources. This approach was complemented with the study of EF values associated with Pb and other potentially toxic elements, and with a previous air masses back trajectories modelling (Plasencia Sánchez et al., 2023). Finally, a health risk assessment was performed for exposure to Pb and other potentially toxic elements to children and adults as a broad estimate of the potential carcinogenic and non-carcinogenic effects across the city.

2. Methodology

2.1. Study site and sampling strategy

The city of Tarragona is located in northeast Spain, on the shore of the Mediterranean Sea. The city and its surrounding area are considered as one of the most industrialised zones in southern Europe (Domínguez-Morueco et al., 2017; Rovira et al., 2024). Local industrial activities comprise (Fig. 1): (A) the north Complex (or Petrochemical area) that includes an oil refinery and several petrochemical industries; (B) the northwest Constantí industrial estate that includes a Hazardous Waste Incinerator (HWI); (C) the south Complex, comprising several chemical industries; (D) the industrial harbour and, (E) the southeast Riu Clar estate, that includes a Municipal Solid Waste Incinerator (MSWI). In the framework of a project assessing children's exposure to indoor (Sánchez-Soberón et al., 2019) and outdoor (Plasencia Sánchez et al., 2023) PM, fourteen schools (Fig. 1) were selected to perform air quality sampling during two seasonal campaigns (cold and warm seasons; December 2016 to March 2017 and September to October 2017). These schools are all located ~2 km away from the four main industrial activities, except location #1, which, being more than 6 km away from any industrial activity, was also selected, and expected to represent the local background. A total of 75 Quartz microFiber Filters (QFF) were collected using high volume air samplers, 25 for each PM size fraction: coarse (PM_{10}), fine ($PM_{2.5}$) and submicron (PM_1) particles (see details of equipment and methodology in Plasencia Sánchez et al., 2023). In addition, 9 samples (M1-M9) from anthropogenic sources were obtained: 3 collected at potential local PM sources (M1, M4, M6) and 6 blind samples (M2, M3, M5, M7-M9) provided by the Tarragona

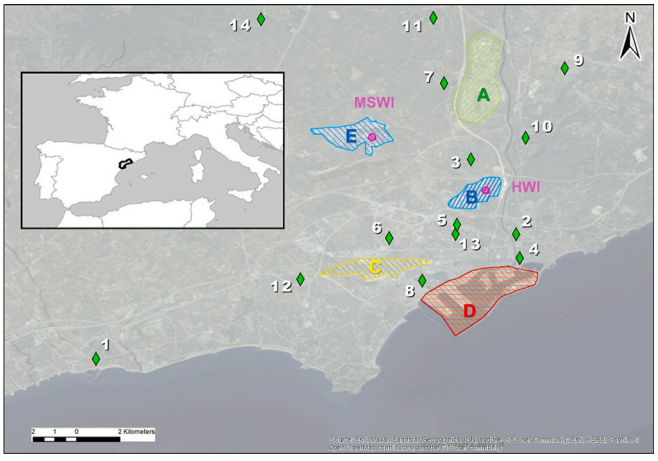

Fig. 1. Sampling points. School's location and ID number (#1 to #14) sampled by Plasencia Sánchez et al. (2023) are marked with green diamonds. The closest industrial estates in Tarragona are also shown: (A) the North Complex (or Petrochemical); (B) the Constantí industrial estate, which contains a Hazardous Waste Incinerator (HWI) (pink circle); (C) the South Complex; and (D) the industrial harbour and (E) the RiuClar estate, where the Municipal Solid Waste Incinerator (MSWI) is also pointed with a pink circle. The base map (World Imagery – Clarity) was obtained from ArcGIS10.2. (For interpretation of the references to colour in this figure legend, the reader is referred to the web version of this article.)

Chemical Business Association (*Associació Empresarial Química de Tarragona*; AEQT — Associació Empresarial Química de Tarragona, 2024). See Table A1 for additional information.

2.2. Pb concentrations and isotope ratios

All samples were prepared in a clean laboratory (class-100) and measured for both Pb concentration and Pb isotope ratios at the Geotop laboratory in Montreal (UQAM) following the procedure described in Widory et al. (2010). In brief, a 6-mm diameter piece of the filter was cut and placed in a Savilex Teflon beaker and leached with aqua regia (HNO_3 + 3 HCl), then, Pb concentrations were measured by ICP-MS (iCAP-Q, ThermoScientific). For Pb quantification, the limit of detection (25 ng/L) was defined as three times the standard deviation of the blanks. For isotope measurements, each solution was purified on an anion exchange resin (BioRad AG1X-8, 200–400 mesh) in a HBr/HCl medium (adapted from Manhes et al., 1978). After chemical purification, samples were diluted in a 2 % HNO_3 solution doped with thallium (Tl) to correct for the mass bias (Belshaw et al., 1998; Woodhead, 2002) on a MC-ICP-MS (NuPlasma II), normalizing to the international standard NBS-981. An internal standard (CGPB-1) was also measured for monitoring the long-term stability ($^{208}Pb/^{204}Pb$ = 37.98 ± 0.02; $^{207}Pb/^{204}Pb$ = 15.698 ± 0.007; $^{206}Pb/^{204}Pb$ = 18.592 ± 0.008; $^{206}Pb/^{207}Pb$ = 1.1844 ± 0.0002; n = 50; 2σ). Procedural blanks were measured by isotope dilution and yielded 0.4 pg of Pb, associated with average $^{208}Pb/^{204}Pb$ = 37.65 ± 0.05; $^{207}Pb/^{204}Pb$ = 15.59 ± 0.02; $^{206}Pb/^{204}Pb$ = 18.18 ± 0.02; $^{206}Pb/^{207}Pb$ = 1.175 ± 0.025 (n = 6; 2σ).

2.3. Other metals concentrations

For each sample, the content of 55 chemical elements, including As, Ca, Cd, Co, Cr, Cu, Fe, K, Mg, Mn, Sb, Sr, Ti, V and Zn, was previously reported elsewhere (Plasencia Sánchez et al., 2023). The detailed description of the methodology followed can be found in Rovira et al. (2018).

2.4. Enrichment Factors (EF)

Enrichment Factors (EF) were calculated using the following equation (e.g. Rahn, 1967; Sun et al., 2014):

$$EF = (C_i/C_{Fe})_{sample} \Big/ (C_i/C_{Fe})_{UCC} \quad (1)$$

where C_i and C_{Fe} are the concentration of the considered element and the conservative element (Fe in our study), respectively, measured in the sample or in the Upper Continental Crust (UCC). We considered the following UCC elemental abundances (expressed in mg/kg or μg/g or ppm): 2, 41,500, 0.15, 25, 102, 66.5, 56,300, 20,900, 23,300, 950, 14, 0.2, 370, 5650, 120 and 70 for As, Ca, Cd, Co, Cr, Cu, Fe, K, Mg, Mn, Pb, Sb, Sr, Ti, V and Zn, respectively (Haynes, 2016). EF are then categorized depending on their value (Chen et al., 2007): no enrichment (EF < 1); minor enrichment (1 < EF < 3); moderate enrichment (3 < EF < 5); moderately severe enrichment (5 < EF < 10); severe enrichment (10 < EF < 25), very severe enrichment (25 < EF < 50); and extremely severe enrichment (EF > 50).

2.5. Potential sources of atmospheric Pb

In addition to the Pb isotope characterization of the local emission sources (M1-M9 samples in Table A3), we considered a set of source values encountered in environments similar to Tarragona (S1-S5 in Table 1) and reference values (R1-R4 in Table 1) from the literature. These sources of atmospheric Pb include a geogenic source in the country: NW Spanish Pb ores (S1) that, as discussed in Arias et al. (1996), show more radiogenic (defined as excess in ^{206}Pb and ^{208}Pb, i.e., higher $^{206}Pb/^{204}Pb$ and $^{208}Pb/^{204}Pb$ ratios) Pb IRs than those predicted for UCC by crustal Pb evolution models (Zartman and Doe, 1981; Ludwig et al., 1989).

Table 1
Pb isotope characteristics for selected sources (S1-S5) and reference values (R1-R4) of atmospheric Pb. Mean value and standard deviation (in brackets) are showed for each considered Pb IR. n = number of values.

Source/Reference value (reference)	Context	Material	n	$^{208}Pb/^{204}Pb$	$^{207}Pb/^{204}Pb$	$^{206}Pb/^{204}Pb$	$^{208}Pb/^{207}Pb$	$^{206}Pb/^{207}Pb$	$^{204}Pb/^{207}Pb$
S1 - NW Spanish ores (a)	Galenas	raw	6	38.5 (0.3)	15.76 (0.08)	18.07 (0.07)	2.44 (<0.01)	1.15 (<0.01)	0.06 (<0.01)
	Sulfosalts	raw	6	39.0 (0.5)	15.8 (0.2)	18.4 (0.1)	2.46 (<0.01)	1.16 (<0.01)	0.06 (<0.01)
S2 - Steel Industry (b)	Metallurgy plant	PM_{10}	–	38.76	15.82	19.34	2.45	1.22	0.06
		$PM_{2.5}$	–	38.46	15.79	19.05	2.44	1.21	0.06
		PM_1	–	38.20	15.74	18.80	2.43	1.19	0.06
S3 – MSWI (c,d)	Paris (cold)	fly ash	3	37.95 (0.02)	15.60 (<0.01)	18.02 (<0.01)	2.43 (<0.01)	1.15 (<0.01)	0.06 (<0.01)
	Paris (warm)	fly ash	3	37.87 (0.02)	15.60 (<0.01)	17.93 (0.02)	2.43 (<0.01)	1.15 (<0.01)	0.06 (<0.01)
S4 – EGU (e)	Coal-fired	fly ash	–	38.87	15.62	18.91	2.49	1.21	0.06
S5 – Road traffic (b)	Diesel and leaded gasoline fleet	PM_{10}	–	37.40	15.58	17.62	2.40	1.13	0.06
		PM_1	–	37.50	15.57	17.69	2.41	1.14	0.06
R1 – Coal (f,g,h,i,j,k,l)	Anthracite, lignite, bituminous	raw	179–329	38.7 (0.7)	15.6 (0.2)	18.6 (0.6)	2.48 (0.03)	1.19 (0.03)	0.06 (<0.01)
R2 - Central heating (c)	Fuel-oil	fly ash	5	37.9 (0.6)	15.60 (0.03)	18.1 (0.6)	2.43 (0.03)	1.16 (0.03)	0.06 (<0.01)
	Natural Gas	fly ash	5	38.1 (0.4)	15.65 (0.04)	18.3 (0.5)	2.43 (0.02)	1.17 (0.03)	0.06 (<0.01)
	Coal-fired	fly ash	1	38.37	15.66	18.40	2.45	1.18	0.06
R3 – Oldest Earth crust (m)	Devil Canyon, CA,USA	raw	–	29.48	10.3	9.31	2.86	0.90	0.10
R4 – Industrial lead line (n,o)	Broken Hill ores, Australie (n)	raw	–	35.66	15.39	16.00	2.32	1.04	0.06
	Missisipi Valley ores, USA (o)	raw	3	40.0 (0.5)	15.88 (0.03)	21.1 (0.4)	2.52 (0.03)	1.33 (0.02)	0.06 (<0.01)

References: (a) Arias et al., 1996; (b) Véron et al., 1999; (c) Widory et al., 2004; (d) Carignan et al., 2005; (e) Chiaradia et al., 1997; (f) Farmer et al., 1999; (g) Monna et al., 2006; (h) Díaz-Somoano et al., 2007; (i) Díaz-Somoano et al., 2009; (j) Bi et al., 2017; (k) Das et al., 2018; (l) Das et al., 2020; (m) Tatsumoto, 1973; (n) Ostic et al., 1967; (o) Doe and Delevaux, 1972

2.6. Isotope mixing model

The MixSIAR framework in R (Stock and Semmens, 2016) was used for source apportionment based on Pb IRs. This module has been recently used to determine the respective contributions of different sources of Pb bound to PM (e.g. Longman et al., 2018; Chen et al., 2023; Dai et al., 2023). Two sets of Pb IRs were used separately: the $^{206}Pb/^{204}Pb$, $^{207}Pb/^{204}Pb$ and $^{208}Pb/^{204}Pb$ ratios shown in Table 1 were used as input parameters, as described in Longman et al. (2018), to maximize sensitivity in the Pb isotope signatures and because each of the radiogenic Pb isotopes forms through a distinct radioactive chain. Additionally, $^{204}Pb/^{207}Pb$, $^{206}Pb/^{207}Pb$ and $^{208}Pb/^{207}Pb$ ratios were also used as input parameters to compute comparative tests of performance and accuracy (through Epsilon and Gelman-Rubin convergence criteria) in several concentration-independent model runs.

2.7. Carcinogenic and non-carcinogenic health risk

Inhalation is the direct route of human exposure to Pb-enriched particles, whereas indirect exposure includes intake via hand-to-mouth activities of particles settled on food, drinks and outdoor surfaces (ATSDR — Agency for Toxic Substances and Disease Registry, 2023). While PM_{10} tend to deposit in the nasal–pharyngeal region, $PM_{2.5}$ can travel deeply into the respiratory tract and reach lungs. PM_1 can reach the lung alveoli. In this study, the Carcinogenic health risk (CR) via the inhalation exposure to Pb and other potentially toxic elements present in PM_{10}, $PM_{2.5}$ and PM_1 was calculated for children and adults following the United States Environmental Protection Agency (US-EPA) human health risk assessment models (US-EPA — United States Environmental Protection Agency, 1989, 2009). The Hazard Quotient (HQ) and the Hazard Index (HI) were used for evaluating non-carcinogenic risks (US-EPA — United States Environmental Protection Agency, 1989). More details are reported in the supplementary material section A.1.1.

2.8. Data analysis

Statistical analysis was performed using Statgraphics XVII. The dataset was categorized by PM size and campaign. The default significance level was set at $\alpha = 0.05$. Normality was evaluated using the Shapiro-Wilk's test, equality of variances through Levene Test at a *p*-value of 0.05 and difference of means by Mann Whitney *U* test or alternatively by one-way ANalysis Of VAriance (ANOVA) at a p-value of 0.05, by default. All maps were generated using ArcGIS 10.2. The Spatial Analyst toolbox was used for assessing Inverse Distance Weighting interpolation (IDW, Shepard, 1968) for the EF value maps. US-NOAA air masses back-trajectories were obtained by Hybrid Single-Particle Lagrangian Integrated Trajectories (HYSPLIT, Draxler, 1999) model in a previous work (Plasencia Sánchez et al., 2023). Charts were generated using MapPlotLib package in Python 3.10.

3. Results and discussion

3.1. Pb vs. other metals concentrations

Lead concentrations in the Tarragona PM samples and in the potential local emission sources are listed in Table A3 and Table A5, respectively. Pb atmospheric concentrations for all schools (from 2×10^{-5} to 6.87×10^{-3} μg/m^3) remain below the European Union (EU) air quality standard of 0.5 μg/m^3 (Directive 2008/50/EC), the United Kingdom (UK) air quality objective of 0.25 μg/m^3 (Air quality standard 2010) or even the stricter United Stated (US) ambient air Pb limit of 0.15 μg/m^3 (National Ambient Air Quality Standards – review 2016). Fig. A1 shows that while Pb in the PM_{10} fraction is higher than in the others fractions for both sampling seasons, Pb mass concentrations are roughly evenly distributed across each fraction, displaying statistically similar mean values ($p < 0.05$). This suggests that Pb is predominantly present in PM_1, which disfavours an origin via mechanical processes and may rather hint that a chemical process such as combustion (Khan et al., 2021) is the main vector of atmospheric Pb in Tarragona. This hypothesis would agree with the findings of Duan et al. (2012) for the city of Beijing (China) and Moreno et al. (2007) for the city of Puertollano (Spain).

A comparison with other metals (data reported in Plasencia Sánchez et al., 2023) reveals that average Pb concentrations, especially in $PM_{2.5}$, are always lower than those of Cu, Mn and Cr, in stark contrast with what was reported for some Asian cities by Sun et al. (2014) or Chifflet et al. (2018) and references therein. Despite this, Pb accounts for up to 16 % and 9 % of the total metal content during the cold and warm seasons, respectively. As shown in Table A2, Cu/Pb ratios >1 indicate the absence of aerosols of natural origin, whereas higher ratios (e.g., Cu/Pb >10) clearly show that emissions from industrial activities and vehicular fossil fuel combustion prevail in the samples. Some of the samples display V/Pb ratios >1 that indicate that these are strongly influenced by coal combustion (Plasencia Sánchez et al., 2023). Unfortunately, as most Ni concentrations were below the limit of quantification of 0.02 μg/m^3 (Plasencia Sánchez et al., 2023), we could not systematically use the classical V/Ni ratio to assess the influence of shipping traffic. However, for the two annual campaigns ($PM_{2.5}$ in 2001 and PM_{10} in 2004; Table A2) when Alastuey et al. (2007) were able to determine V/Ni ratios in Tarragona PM samples, these were in a good agreement with what is expected for the west Mediterranean basin where the combustion of fuel-oil from power generation units, industrial and shipping represent the main vector of atmospheric V (Querol et al., 2009). Additionally, we observed a decrease in the total metal content from the coast to the mainland (Plasencia Sánchez et al., 2023).

3.2. Enrichment Factors (EF)

As shown in Fig. A2, the EF for As, Ca, Co, K, Mg, V and Zn are mostly categorized as severe or very severe ($50 > EF > 10$) attending to $PM_{2.5}$ results, which strongly suggests an anthropogenic origin. This conclusion is beyond doubt for Pb, together with Cd, Cu and Sb, which reached extremely severe EF in all PM sizes. In the case of Pb, this enrichment was statically higher ($p < 0.05$) in the cold than in the warm campaign for PM_1 samples, which is also observed for V and Zn, pointing to petroleum-derived fuels and oils. This behavior was, however, not observed for $PM_{2.5}$ and PM_{10} samples. The spatial distribution of the Pb enrichment factors (EF_{Pb}) identifies emission hotspots mostly located between the HWI and the harbour estate (Fig. A3). The different size fractions display variability: while $PM_{2.5}$ and PM_1 samples collected in the cold campaign all yield extremely severely enriched EF_{Pb}, for PM_{10}, areas located near the west shoreline in the cold campaign and between the eastern inland and shoreline in the warm campaign are less enriched. Both PM_{10} and PM_1 samples collected in the warm campaign in the close vicinity of school #12 are severely enriched, whereas surrounding areas are less impacted, with moderately severe EF_{Pb}.

3.3. Pb isotope ratios

The ^{204}Pb-normalised Pb IRs (i.e., $^{208}Pb/^{204}Pb$ and $^{206}Pb/^{204}Pb$) are typically used to compare the geochronology of ores for geogenic sources (e.g., Ludwig et al., 1989), while ^{207}Pb-normalised Pb IRs (i.e., $^{208}Pb/^{207}Pb$ and $^{206}Pb/^{207}Pb$), also known as radiogenic ratios, are commonly used to identify some anthropogenic activities (e.g., De la Cruz et al., 2009). The analysis of the distribution of both the non-radiogenic and radiogenic Pb IRs would therefore document the geological age or the activities responsible for the presence of atmospheric Pb.

3.3.1. Description and interpretation of non-radiogenic Pb IRs

The range of values of the $^{208}Pb/^{204}Pb$ and $^{206}Pb/^{204}Pb$ ratios varied according to the PM size fraction for both sampling campaigns (see

Table A5 and Fig. A4). Minimal variation in both ratios was observed in the submicron fraction (PM_1), especially in the cold campaign, whereas a higher variability was observed in the coarse fraction (PM_{10}). When examining the normally distributed PM_1 and $PM_{2.5}$ subsets from the cold season, their $^{208}Pb/^{204}Pb$ mean values (38.01 ± 0.09 and 38.07 ± 0.06, respectively) were significatively distinct ($p < 0.05$) from those of the warm campaign (37.8 ± 0.2 and 37.93 ± 0.02, respectively). In contrast, the mean value of $^{208}Pb/^{204}Pb$ ratios in PM_{10} remained statistically constant ($p > 0.05$) throughout the year, with values of 37.9 ± 0.1 and 37.8 ± 0.3 for the cold and warm campaign, respectively. This suggests that, while a single emission source may have annually shaped Pb in the coarse fraction, for the fine and submicron fractions it may reflect either different sources contributing seasonally or the same sources characterized by seasonally varying contributions.

The outliers for both $^{208}Pb/^{204}Pb$ and $^{206}Pb/^{204}Pb$ ratios correspond mainly to school #4, with the lowest values in the $PM_{2.5}$ and PM_{10} fractions for both campaigns, and to school #12, also with low radiogenic IRs values in the warm PM_{10} fraction. These schools are coincident to the locations having lower anthropogenic influence according to their $EF_{Pb} \leq 50$ (i.e., severe and very severe enrichment areas in Fig. A3). Therefore, these areas may reflect Pb geogenic inputs from external air masses. To further investigate this hypothesis, data were plotted on an EF_{Pb} vs. $^{208}Pb/^{204}Pb$ graph (Fig. A5A). The PM samples exhibiting both $EF_{Pb} \leq 50$ and a low radiogenic $^{208}Pb/^{204}Pb$ ratio include PM_{10} samples from schools #12 and #4 during the warm campaign, as well as those from schools #12, #1 and #8 during the cold campaign. Additionally, PM_1 samples from schools #1 and #10 in the warm campaign fall into this category. The modelled air masses back trajectories for these samples also align with geogenic inputs from external air masses (Fig. A6).

3.3.2. Description and interpretation of radiogenic Pb IRs

In contrast to the non-radiogenic ratios, the radiogenic ratios, $^{206}Pb/^{207}Pb$ and $^{208}Pb/^{207}Pb$, show almost no outliers (Fig. A4). The mean values of the $^{206}Pb/^{207}Pb$ ratio were statistically constant between the cold and warm campaigns: 1.162 ± 0.004 and 1.161 ± 0.003 for PM_1, 1.163 ± 0.003 and 1.161 ± 0.003 for $PM_{2.5}$ and 1.164 ± 0.003 and 1.165 ± 0.005 for PM_{10}, respectively, with only school #14 being an outlier in the warm $PM_{2.5}$ size fraction. These average values align with the $^{206}Pb/^{207}Pb$ range reported for the UCC (1.151 to 1.232, Ray et al., 2024), hinting at probable geogenic inputs. However, they are near to the upper range values observed in the Chinese industrial megacity Tianjin, where reported $^{206}Pb/^{207}Pb$ range for PM_{10} (1.142–1.164) was latter mainly associated to a mixing of emissions from coal combustion (around 50 %, with secondary contribution from a waste incineration power plant), iron and steel plants (~30 %) and road vehicles (~20 %) (Dai et al., 2023). In contrast, our $^{206}Pb/^{207}Pb$ values range out from those reported for $PM_{2.5}$ in another industrial city in northern China, Changzhi (1.088–1.098), where the source apportionment indicated a more evenly distributed mix of pollution sources (Chen et al., 2023).

Therefore, a mixture of various geogenic/anthropogenic sources likely contributed to Pb contamination in the Tarragona PM samples. This is supported by the "mixing plots" (i.e., Pb isotope ratios vs. inverse Pb concentration, e.g. Faure, 1986; Hansmann and Köppel, 2000; Chen et al., 2022) (Fig. A7), which do not display clear linear mixing patterns, further suggesting the contribution of at least three distinct sources with different Pb isotopic compositions in both campaigns.

3.3.3. Potential sources of atmospheric Pb

As shown in Table 1, despite the large heterogeneity in their incinerated waste materials, European Municipal Solid Waste Incinerators (MSWI, S3) exhibit relatively homogenous Pb IRs in their emissions (Komárek et al., 2008). Emissions from coal-fired blast furnaces from the steel industry (S2) and Electrical Generation Units (EGUs, S4) exhibit Pb IRs distinct from those of their parent coal (R1, which represents the world average isotope ratios for mineral coal ores). This distinction strongly suggests that Pb in these emissions does not solely originate from the raw material. R1 is certainly a reference value for Tarragona considering the extensive use of coal for domestic heating and leisure activities (e.g., barbecues during winter and summer) and for fuelling EGUs, industrial furnaces and blast furnaces, which are found within 50 km around Tarragona. However, R1 could not be an appropriate source (input for the mixing model) due to the high variability of its Pb IRs (coefficient of variation, CV ≈ 3 %). In other words, if R1 was considered a geogenic source, its higher CV would result in contributions that would mask S4, and probably also S2, contributions. Thus, in the opposite scenario, considering anthropogenic sources S4 and S2, that display lower variability (CV ≈ 0.5 %), the largest the variability of their contributions the largest the possible geogenic contribution. Values of Pb IRs for central heating systems (R2) vary depending on the type of combusted fuel and cannot be isotopically discriminated due to overlapping ranges (Table 1). Therefore, contribution from R2 is encompassed within the uncertainty of the contribution from other sources combusting the same fuel. Values of Pb IRs associated to road traffic emissions (S5) are in a good agreement with the isotope ranges reported for the different gasoline types in the literature (Véron et al., 1999). The commonly accepted "industrial lead line" (R4) represents a mixture of materials ranging from the low radiogenic Pb Australian deposits (e.g., Broken Hill ores) to the more radiogenic Pb Mississippi Valley type ores (USA), which were both used for almost a century in the production of leaded gasoline around the world (Komárek et al., 2008). We, thus, refer to this line also as "leaded gasoline line". As that S2 lies along R4, most of the legacy of leaded gasoline (contaminated soil resuspension) is likely included in the variability of S2 contribution. Finally, Devil Canyon troilite, USA (R3) represents a time reference (4.55 billion years-old) in the classic dual $^{208}Pb/^{204}Pb$ vs. $^{206}Pb/^{204}Pb$ diagram (Doe and Stacey, 1974).

3.3.4. Pb source identification in samples

The use of the bivariate isotope plots comparing the Pb IRs of the PM samples with those of the potential local (blind) emission samples (M1-M9, Table A3), known sources, and reference materials reported in the literature (Table 1) may aid constraining contamination sources. First, the Pb IRs of the potential local emission sources were compared to those of known sources and reference materials. In the non-radiogenic Pb ratios plot (Fig. 2A-B) the sample from the coal harbour (M4) is consistently positioned similar to the coal ore (R1) or the coal-fired EGU (S4) emission sources. The diesel tailpipe sample (M1) and the blind sample M2 are positioned near the road traffic source (S5). M7 (blind) is closely associated with the municipal solid waste incineration (S3), whereas M9 is clearly distinct to the others, exhibiting the lowest values for both non-radiogenic Pb IRs (Fig. 2A). M3, M5, M6 and M8 have Pb IRs values that fall between those of M1-M2 and M4. On the other hand, according to radiogenic Pb IRs (Fig. 2C-D), all potential local (blind) source samples, including M9, plot within the range of road traffic (S5) and coal-fired EGU emissions (S4), with potential contributions from NW Spanish ores (S1) in source samples such as M3 and M6 that exhibited $EF_{Pb} \leq 50$ (Fig. A5B), as well as from the global average for coal ore (R1).

Similar to the local emission samples, most of the results for the PM samples shown in Fig. 2, independently of their fraction size and sampling season, plot within the Pb IRs measured for sources S5 (road traffic) and S4 (coal-fired EGUs). Either for non-radiogenic (Fig. 2A-B) or radiogenic (Fig. 2C-D) Pb IRs, most of the PM samples are clearly aligned above the industrial lead line/leaded gasoline line (orange dotted line), discarding a direct contribution from leaded gasoline after its phase-out in 2001 in Spain, as seen in recent studies (e.g. Das et al., 2018). Despite this, soil resuspension, through Pb NW Spain ores (S1), steel industry emissions (S2) and MSWI emissions (S3), could have exerted great influence on how the different size-segregated PM are dispersed along the whole mixing area in the bivariate isotope plots.

Only in the case of non-radiogenic Pb IRs, some PM_{10} samples, collected both in the cold and warm campaigns, yielded low isotope

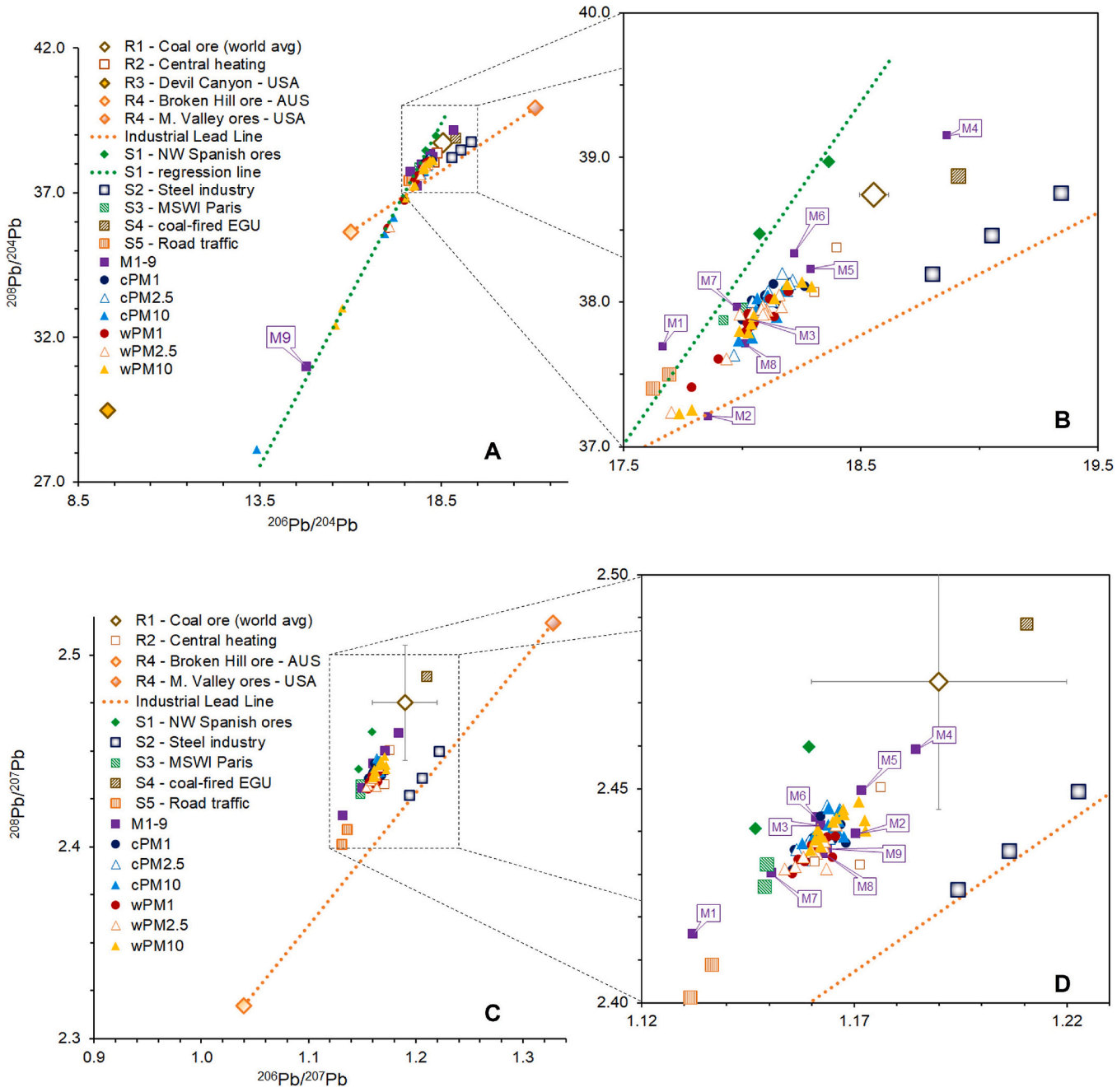

Fig. 2. Bivariate isotope plots of non-radiogenic (A and B) and radiogenic (C and D) Pb IRs for the size-segregated PM samples (Table A5), the potential end-members (local (blind) emission sources –M1-M9, Table A3– and literature end-members – S1-S5, Table 1–) and reference values (R1-R4, Table 1). Prefixes "c" and "w" stand for the cold and warm seasons, respectively. When not shown, uncertainties are smaller than the symbols.

ratios below the leaded gasoline line, and in line with blind source M9 (Fig. 2A). These low radiogenic Pb IRs are also lower than those determined from the conventional modern continental crust model (17.29–19.33 for $^{206}Pb/^{204}Pb$ and 38.56–39.06 for $^{208}Pb/^{204}Pb$, Zartman and Doe, 1981), which indicates that they derive from a distinct geologic reservoir. They all plot on an extended line connecting the galena and sulfosalts Pb isotope signatures of the NW Spanish ores (S1, green dotted line in Fig. 2A). In accordance with what we discussed previously for the EF_{Pb} vs. $^{206}Pb/^{204}Pb$ plot (Fig. A5A), we hypothesise that the low isotope ratio of these samples is indicative of a geogenic origin by transport and/or resuspension of weathered soil materials (Chen et al., 2022; Dausmann et al., 2019). This hypothesis is supported by the fact that the four lowest values of $^{208}Pb/^{204}Pb$ ratio in the cold campaign (PM_{10} from schools #1, #4, #8 and #12) occurred when air masses from NW of Spain were present in Tarragona (Fig. A7). During the warm campaign, most of the lowest non-radiogenic Pb IRs values (mainly PM_{10} from schools #4 and #12, and PM_1 from school #1 and #10) were coincident with simultaneous occurrence of both air masses intrusions from NW of Spain and others from the Balearic Islands (Fig. A7).

In summary, the bivariate isotope plots suggest that, along with some geogenic contributions, anthropogenic sources such as MSWI, EGU, and road traffic —but not leaded gasoline—directly contributed to Pb contamination. Consequently, for source apportionment, the set of sources S1-S5, which form a convex polygon on the bivariate isotope plots, were considered as end-member sources in our Bayesian mixing model.

3.4. Atmospheric Pb source apportionment

To address the wide range of values for the $^{208}Pb/^{204}Pb$ isotope ratio, we categorized the data into subsets as follows: D90 included the 10 lowest $^{208}Pb/^{204}Pb$ values, D09 the next 4 lowest ones, and D01 the remaining data. D00 was defined as D01 + D09 + D90 (whole dataset), whereas D10 included only D01 and D09.

First, using increasing computational iterations from the lowest (Test) to the highest (VeryLong) in the MixSIAR interface (following the protocol described in Longman et al., 2018), we evaluated several mixing scenarios. These scenarios incorporated different datasets (D01, D10 or D00) and categories (campaigns, PM fractions, or both), always considering the five sources S1-S5 (see Table A6 and Fig. A8). Instead of using the 90th percentile (e.g. Longman et al., 2018) or the minimum-maximum range criteria (e.g. Ray and Das, 2023), we chose to express the highest apportion probability for each emission source by the means of its interquartile range value (Plasencia Sánchez et al., 2023). This was motivated by both its statistical significance and its acotated range values, overcoming any possible small source bias.

No significant differences were observed in terms of uncertainty reduction (value of mean or interquartile range for each epsilon) or total source contributions (the sum of interquartile range for each source) when using the $^{206}Pb/^{204}Pb$, $^{207}Pb/^{204}Pb$ and $^{208}Pb/^{204}Pb$ ratios as tracers. However, excluding the $^{207}Pb/^{204}Pb$ ratio and only considering the other 2 ratios (i.e., $^{206}Pb/^{204}Pb$ and $^{208}Pb/^{204}Pb$), improved the model performance by over 15 %. Additionally, normalizing isotope ratios to ^{207}Pb instead of ^{204}Pb reduced uncertainties by half and nearly doubled the total contributions.

Source contributions in the PM samples of the three size fractions (PM_1, $PM_{2.5}$ and PM_{10}) were determined using several mixing models with both ^{204}Pb- and ^{207}Pb-normalised Pb isotope ratios. Calculated source contributions for the most relevant scenario, which combines tracers and computational efforts, are presented in Fig. 3 Detailed run configurations, results and convergence evaluations are provided in Table A6.

Results indicate that emissions from waste incinerators (S3) are generally the major contributor for all fractions and seasons, with contributions of at least 20 % and up to 60 %. Although S3 corresponds to fly ash samples from a MSWI, due to the potentially toxic elements profile, we consider that in Tarragona both the MSWI and the HSWI contributed to Pb contamination. Second in importance, road traffic (S5) contributes to 20–40 % for all PM fractions, with slightly higher contributions for the fine fraction during the warm season, in agreement with previous findings (e.g., Oliveira et al., 2010). Contributions from coal-fired EGUs (S4) are rather constant between fractions and seasons, generally accounting for 15–35 %, with values slightly increasing with the size fraction ($PM_1 < PM_{2.5} < PM_{10}$). Finally, NW Spanish ores (S1) and industrial activities (S2) each contribute <10 % all fractions, with S1 exhibiting relative higher contributions during the cold campaign compared to the warm campaign.

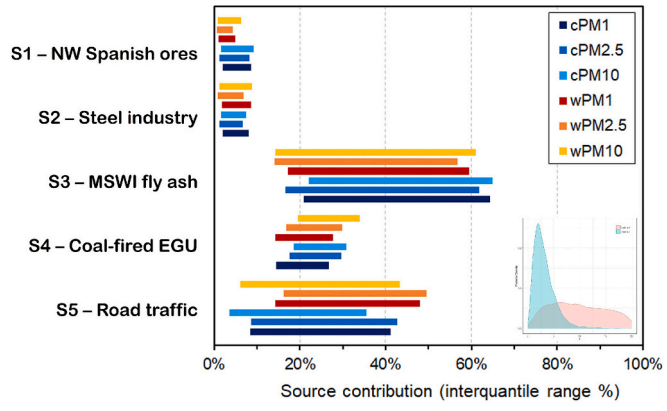

Fig. 3. Apportioned source contributions, segregated by PM size and seasonality. Contributions were determined according to the best performance (lowest mean uncertainties ε_1 and ε_2) scenario in MixSIAR, using $^{206}Pb/^{207}Pb$ and $^{208}Pb/^{207}Pb$ ratios as tracers and *normal* longitude chains for computing effort. Prefix "c" in the legend box and bluish bars refer to the cold sampling campaign, whereas "w" and reddish bars correspond to the warm sampling campaign. Uncertainties are showed at the right down corner.

3.5. Health risk assessment

Carcinogenic health risk values were broadly estimated for both children and adults (as detailed in A.2.1). In Table 2 they are presented as the probable number of additional cancer cases per million of people, under the worst-case scenario (24 h outdoor exposure). On average, CR values were higher during the cold than the warm campaign for all metals, with the exception of Co and Ni. Generally, the calculated CRs increased with the size fractions ($PM_1 < PM_{2.5} < PM_{10}$). Notably, the CRs calculated for $PM_{2.5}$ were similar to the overall averages, highlighting the importance of this fraction. In most cases, CR values were below the threshold of 10^{-4} (i.e., 100 case per million people), and thus can be considered as acceptable, except for Cr in adults. Indeed, Cr and to a lesser extent Co, As, Cd or Ni were the metals associated with the highest number of additional cancer cases. In contrast, Pb appeared to have a lower impact in the city, with a maximum of 3 additional adult cancer cases per million of people (Table 2).

The CRs estimated in this work align closely with those of a previous study conducted in Tarragona for PM_{10} (Rovira et al., 2024). Notably, obtained Pb CRs are comparable to those reported for the city of Madrid (Spain) (PM_{10}; De Miguel et al., 2007), which has a population of 3 million, 20 times higher than that of Tarragona. Our PB CR values are roughly half of the values observed in Nanjing, China (8 million inhabitants; TSP and $PM_{2.5}$; Hu et al., 2012), and about one third of those reported for Chengdu, China (16 million inhabitants; $PM_{2.5}$; Li et al., 2016).

4. Conclusions

In this study, we assessed the contributions of various Pb air pollution sources to size-segregated PM (PM_1, $PM_{2.5}$ and PM_{10}) samples in the complex industrial and urban environment of Tarragona. The Pb IRs profiles in the PM samples for the two seasonal campaigns revealed a strong anthropogenic contamination, a finding corroborated by the study of the metal EF values and their spatial distributions. Despite this, some PM_{10} samples exhibited extremely low $^{208}Pb/^{204}Pb$ isotope ratios, which were attributed to a geogenic origin, a conclusion further supported by the corresponding modelled air mass back trajectories.

Pb source apportionment using both ^{204}Pb- and ^{207}Pb-normalised isotope ratios within a Bayesian mixing model identified waste incinerators (MSWI and HWI) as the primary contributors to Pb air pollution (accounting for at least 10 % in PM_{10} and up to 60 % in both $PM_{2.5}$ and PM_1), followed by road traffic and coal-fired EGUs (contributing up to 40 % and 20 %, respectively, in all PM fractions). Geogenic particles (NW Spanish ores and possible soil resuspension) contributed less than 10 % in all PM fractions.

Linked to MSWI and HWI emissions, carcinogenic and non-carcinogenic health risks were assessed for various potentially toxic elements and PM sizes. Our findings suggest that the $PM_{2.5}$ size fraction serves as a reliable proxy for estimating the overall metal-related health impact. Although the estimated probable additional cancer cases (e.g., 3 additional cancer cases for adults per million of people due to Pb exposure) were low in absolute numbers, they are comparable to those observed in much more populated cities, indicating a notable health concern for Tarragona.

Table 2
Carcinogenic health risk (CR) associated to metal exposure by inhalation. CR is expressed as the probable number of additional cancer cases per million of people during their lifetime.

		Overall average		PM_1		$PM_{2.5}$		PM_{10}	
Population	Element	cold	warm	cold	warm	cold	warm	cold	warm
Children	As	0.9	0.5	0.3	0.1	0.9	0.4	1.6	0.9
	Cd	0.7	0.1	0.5	0.0	0.5	0.1	1.1	0.2
	Co	1.2	5.7	1.3	9.5	0.9	3.8	1.6	3.8
	Cr	69.9	48.2	19.4	69.4	84.8	31.4	105.5	43.8
	Ni	0.3	0.6	0.5	0.6	0.1	0.6	0.2	0.7
	Pb	0.3	0.2	0.2	0.1	0.3	0.1	0.5	0.3
Adults	As	6.2	3.2	1.8	0.8	6.0	2.7	10.7	6.2
	Cd	4.6	0.7	3.1	0.3	3.6	0.7	7.0	1.0
	Co	8.3	38.3	8.4	63.6	5.7	25.6	10.6	25.6
	Cr	466.0	321.3	129.2	462.9	565.7	209.4	703.2	291.72
	Ni	1.85	4.28	3.07	3.69	0.99	4.17	1.48	5.0
	Pb	2.28	1.02	1.65	0.47	2.08	0.90	3.10	1.7

CRediT authorship contribution statement

Edson Plasencia Sánchez: Writing – original draft, Visualization, Methodology, Investigation, Formal analysis, Data curation, Conceptualization. **Mònica Rosell:** Writing – review & editing, Supervision, Methodology, Conceptualization. **Clara Torrentó:** Writing – review & editing, Supervision, Methodology, Conceptualization. **Francisco Sánchez-Soberón:** Writing – review & editing, Investigation, Data curation. **Joaquim Rovira:** Writing – review & editing, Methodology, Investigation, Data curation. **Jordi Sierra:** Writing – review & editing, Investigation, Data curation. **Marta Schuhmacher:** Funding acquisition, Conceptualization. **Albert Soler:** Project administration, Funding acquisition, Conceptualization. **David Widory:** Writing – review & editing, Supervision, Methodology, Investigation, Data curation, Conceptualization.

Declaration of competing interest

None.

Acknowledgements

The present research work was funded by UltraPAR [CTM 2015-65303-P], REMEDIATION [CGL2014-57215-C4-1-R] and PACE [CGL2017-87216-C4-1-R] projects, all funded by MICIU/AEI/10.13039/501100011033/ and by ERDF A way of making Europe. This work was also partly supported by the *Generalitat de Catalunya* through the Consolidate Research Group [2021-SGR-00308] and E. Plasencia Sánchez Predoctoral Fellowship [2020 FISDU 00567]. He was earlier supported from the Peruvian Government loan "Reto Excelencia" [036–2015]. We also thank the AEQT and the Directive Boards of the fourteen educative centers involved in the present study for their kind cooperation.

Appendix A. Supplementary data

Supplementary data to this article can be found online at https://doi.org/10.1016/j.atmosres.2025.107939.

Data availability

Data will be made available on request.

References

AEQT — Associació Empresarial Química de Tarragona, 2024, May 1. Qui Som. http://aeqtonline.com.

Alastuey, A., Moreno, N., Querol, X., Viana, M., Artiñano, B., Luaces, J.A., Basora, J., Guerra, A., 2007. Contribution of harbour activities to levels of particulate matter in a harbour area: Hada Project-Tarragona Spain. Atmos. Environ. 41, 6366–6378.

Álvarez-Iglesias, P., Rubio, B., Millos, J., 2012. Isotopic identification of natural vs. anthropogenic lead sources in marine sediments from the inner Ría de Vigo (NW Spain). Sci. Total Environ. 437, 22–35.

Amelin, Y.V., Neymark, L.A., 1998. Lead isotope geochemistry of Paleoproterozoic layered intrusions in the eastern Baltic shield: Inferences about magma sources and U-Th-Pb fractionation in the crust-mantle system. Geochim. Cosmochim. Acta 62, 493–505.

Anaman, R., Peng, C., Jiang, Z., Amanze, C., Fosua, B.A., 2024. Distinguishing the contributions of different smelting emissions to the spatial risk footprints of toxic elements in soil using PMF, Bayesian isotope mixing models, and distance-based regression. Sci. Total Environ. 933, 173153.

Arias, D., Corretgé, L.G., Suárez, O., Villa, L., Cuesta, A., Gallastegui, G., 1996. Lead and sulfur isotope compositions of the Ibias gold vein system (NW Spain): genetic implications. Econ. Geol. 91, 1292–1297.

ATSDR — Agency for Toxic Substances and Disease Registry, 2023, October 10. Toxicology Curriculum for Communities Trainer's Manual. Module 2. https://www.atsdr.cdc.gov/training/toxmanual.

Audi, G., Bersillon, O., Blachot, J., Wapstra, A.H., 2003. NUBASE: a database of nuclear and decay properties. Nucl. Phys. 729, 3–128.

Ault, W.U., Senechal, R.G., Erlebach, W.E., 1970. Isotopic composition as a natural tracer of lead in the environment. Environ. Sci. Technol. 4, 305–313.

Belshaw, N.S., Freedman, P.A., O'nions, R.K., Frank, M., Guo, Y., 1998. A new variable dispersion double-focusing plasma mass spectrometer with performance illustrated for Pb isotopes. Int. J. Mass Spectrom. 181 (1–3), 51–58.

Bi, X.Y., Li, Z.G., Wang, S.X., Zhang, L., Xu, R., Liu, J.L., Yang, H.M., Guo, M.Z., 2017. Lead isotopic compositions of selected coals, Pb/Zn ores and fuels in China and the application for source tracing. Environ. Sci. Technol. 51 (22), 13502–13508.

Bird, G., Brewer, P.A., Macklin, M.G., Nikolova, M., Kotsev, T., Mollov, M., Swain, C., 2010. Pb isotope evidence for contaminant-metal dispersal in an international river system: the lower Danube catchment, Eastern Europe. Appl. Geochem. 25, 1070–1084.

Carignan, J., Libourel, G., Cloquet, C., Le Forestier, L., 2005. Lead isotopic composition of fly ash and flue gas residues from municipal solid waste combustors in France: implications for atmospheric lead source tracing. Environ. Sci. Technol. 39 (7), 2018–2024.

Chang, C., Han, C., Han, Y., Hur, S.D., Lee, S., Motoyama, H., Hou, S., Hong, S., 2016. Persistent Pb pollution in central East Antarctic snow: a retrospective assessment of sources and control policy implications. Environ. Sci. Technol. 50 (22), 12138–12145.

Chen, C.W., Kao, C.M., Chen, C.F., Dong, C.D., 2007. Distribution and accumulation of heavy metals in the sediments of Kaohsiung Harbor, Taiwan. Chemosphere 66, 1431–1440.

Chen, Z., Ding, Y., Jiang, X., Duan, H., Ruan, X., Li, Z., Li, Y., 2022. Combination of UNMIX, PMF model and Pb-Zn-Cu isotopic compositions for quantitative source apportionment of heavy metals in suburban agricultural soils. Ecotoxicol. Environ. Saf. 234, 113369.

Chen, H., Yan, Y., Hu, D., Peng, L., Wang, C., 2023. High contribution of vehicular exhaust and coal combustion to PM2. 5-bound Pb pollution in an industrial city in North China: an insight from isotope. Atmos. Environ. 294, 119503.

Chiaradia, M., Chenhall, B.E., Depers, A.M., Gulson, B.L., Jones, B.G., 1997. Identification of historical lead sources in roof dusts and recent lake sediments from an industrialized area: indications from lead isotopes. Sci. Total Environ. 205 (2–3), 107–128.

Chifflet, S., Amouroux, D., Bérail, S., Barre, J., Van, T.C., Baltrons, O., Brune, J., Dufour, A., Guinot, B., Mari, X., 2018. Origins and discrimination between local and regional atmospheric pollution in Haiphong (Vietnam), based on metal (loid) concentrations and lead isotopic ratios in PM 10. Environmental Science and Pollution Research 25, 26653–26668.

CIAAW - Commission on Isotopic Abundances and Atomic Weights, International Union of Pure and Applied Chemestry, 2024, July 4. Isotopic Compositions of the Elements 2021. http://www.ciaaw.org.

Dai, W.J., Li, X.D., Fu, Y.C., Ding, S.Y., Li, Q.K., Zhao, Z.Q., 2023. Identification and contribution of potential sources to atmospheric lead pollution in a typical megacity:

insights from isotope analysis and the Bayesian mixing model. Sci. Total Environ. 892, 164567.
Das, R., Mohtar, A.T.B.M., Rakshit, D., Shome, D., Wang, X., 2018. Sources of atmospheric lead (Pb) in and around an Indian megacity. Atmos. Environ. 193, 57–65.
Das, A., Kumar, R., Patel, S.S., Saha, M.C., Guha, D., 2020. Source apportionment of potentially toxic elements in street dust of a coal mining area in Chhattisgarh, India, using multivariate and lead isotopic ratio analysis. Environ. Monit. Assess. 192, 1–14.
Dausmann, V., Gutjahr, M., Frank, M., Kouzmanov, K., Schaltegger, U., 2019. Experimental evidence for mineral-controlled release of radiogenic Nd, Hf and Pb isotopes from granitic rocks during progressive chemical weathering. Chem. Geol. 507, 64–84.
De la Cruz, M.T., Laborda, F., Callén, M.S., López, J.M., Mastral, A.M., 2009. Study of Pb sources by Pb isotope ratios in the airborne PM_{10} of Zaragoza, Spain. J. Environ. Monit. 11 (11), 2052–2057.
De Miguel, E., Iribarren, I., Chacon, E., Ordonez, A., Charlesworth, S., 2007. Risk-based evaluation of the exposure of children to trace elements in playgrounds in Madrid (Spain). Chemosphere 66 (3), 505–513.
Deboudt, K., Flament, P., Weis, D., Mennessier, J.P., Maquinghen, P., 1999. Assessment of pollution aerosols sources above the Straits of Dover using lead isotope geochemistry. Sci. Total Environ. 236, 57–74.
Díaz-Somoano, M., Suárez-Ruiz, I., Alonso, J.I.G., Encinar, J.R., López-Antón, M.A., Martínez-Tarazona, M.R., 2007. Lead isotope ratios in Spanish coals of different characteristics and origin. Int. J. Coal Geol. 71 (1), 28–36.
Díaz-Somoano, M., Kylander, M.E., López-Antón, M.A., Suárez-Ruiz, I., Martínez-Tarazona, M.R., Ferrat, M., Kober, B., Weiss, D.J., 2009. Stable lead isotope compositions in selected coals from around the world and implications for present day aerosol source tracing. Environ. Sci. Technol. 43 (4), 1078–1085.
Dickin, A.P., 1995. Radiogenic Isotope Geology. Cambridge University Press, United Kingdom.
Dietrich, M., Krekeler, M.P., Kousehlar, M., Widom, E., 2021. Quantification of Pb pollution sources in complex urban environments through a multi-source isotope mixing model based on Pb isotopes in lichens and road sediment. Environ. Pollut. 288, 117815.
Doe, B.R., Delevaux, M.H., 1972. Source of lead in Southeast Missouri galena ores. Econ. Geol. 67 (4), 409–425.
Doe, B.R., Stacey, J.S., 1974. The application of lead isotopes to the problems of ore genesis and ore prospect evaluation: a review. Econ. Geol. 69 (6), 757–776.
Domínguez-Morueco, N., Augusto, S., Trabalón, L., Pocurull, E., Borrull, F., Schuhmacher, M., Domingo, J.L., Nadal, M., 2017. Monitoring PAHs in the petrochemical area of Tarragona County, Spain: comparing passive air samplers with lichen transplants. Environ. Sci. Pollut. Res. 24, 11890–11900.
Draxler, Roland R., 1999. HYSPLIT Radiological Transport and Dispersion Model Implementation on NCEP Cray. U.S. Department of Commerce, National Oceanic and Atmospheric Administration, National Weather Service, Office of Meteorology, Science Division, Silver Spring, Maryland.
Duan, J., Tan, J., Wang, S., Hao, J., Chai, F., 2012. Size distributions and sources of elements in particulate matter at curbside, urban and rural sites in Beijing. J. Environ. Sci. 24 (1), 87–94.
Farmer, J.G., Eades, L.J., Graham, M.C., 1999. The lead content and isotopic composition of British coals and their implications for past and present releases of lead to the UK environment. Environ. Geochem. Health 21, 257–272.
Faure, G., 1986. Principles of Isotope Geology, 2nd edition. Wiley, New York, p. 589.
Faure, G., Mensing, T.M., 2005. Isotopes: Principles and Applications, 3rd edition. Wiley-Blackwell, United States of America.
Hansmann, W., Köppel, V., 2000. Lead-isotopes as tracers of pollutants in soils. Chem. Geol. 171, 123–144.
Haynes, W.M. (Ed.), 2016. CRC Handbook of Chemistry and Physics, 97th edition. CRC Press, Boca Raton, FL, pp. 14–17.
Hu, X., Zhang, Y., Ding, Z., Wang, T., Lian, H., Sun, Y., Wu, J., 2012. Bioaccessibility and health risk of arsenic and heavy metals (Cd, Co, Cr, Cu, Ni, Pb, Zn and Mn) in TSP and PM2. 5 in Nanjing, China. Atmos. Environ. 57, 146–152.
IARC - International Agency for Research on Cancer, 2013. Outdoor air pollution, Monographs on the Evaluation of Carcinogenic Risks to Humans, Vol.109.
Kampa, M., Castanas, E., 2008. Human health effects of air pollution. Environ. Pollut. 151, 362–367.
Khan, J.Z., Sun, L., Tian, Y., Dai, Q., Hu, T., Feng, Y., 2021. Size distribution of ambient particulate matter and its constituent chemical species involving saccharides during early summer in a Chinese megacity. Front. Environ. Sci. 9, 659329.
Komárek, M., Ettler, V., Chrastný, V., Mihaljevič, M., 2008. Lead isotopes in environmental sciences: a review. Environ. Int. 34, 562–577.
Kylander, M.E., Klaminder, J., Bindler, R., Weiss, D.J., 2010. Natural lead isotope variations in the atmosphere. Earth Planet. Sci. Lett. 290, 44–53.
Lanphear, B.P., Dietrich, K.N., Berger, O., 2003. Prevention of lead toxicity in US children. Ambul. Pediatr. 3 (1), 27–36.
Lanphear, B.P., Hornung, R., Khoury, J., Yolton, K., Baghurst, P., Bellinger, D.C., Canfield, R.L., Dietrich, K.N., Bornschein, R., Greene, T., Rothenberg, S.J., Needleman, H.L., Schnaas, L., Wasserman, G., Graziano, J., Roberts, R., 2005. Low-level environmental lead exposure and children's intellectual function: an international pooled analysis. Environ. Health Perspect. 113 (7), 894–899.
Li, Y., Zhang, Z., Liu, H., Zhou, H., Fan, Z., Lin, M., Wu, D., Xia, B., 2016. Characteristics, sources and health risk assessment of toxic heavy metals in PM 2.5 at a megacity of Southwest China. Environ. Geochem. Health 38, 353–362.
Longman, J., Veres, D., Ersek, V., Phillips, D.L., Chauvel, C., Tamas, C.G., 2018. Quantitative assessment of Pb sources in isotopic mixtures using a Bayesian mixing model. Sci. Rep. 8 (1), 6154.
Loomis, D., Grosse, Y., Lauby-Secretan, B., El Ghissassi, F., Bouvard, V., Benbrahim-Tallaa, L., Guha, N., Baan, R., Mattock, H., Straif, K., 2013. The carcinogenicity of outdoor air pollution. Lancet Oncol. 4, 1262–1263.
Ludwig, K.R., Vollmer, R., Turi, B., Simmons, K.R., Perna, G., 1989. Isotopic constraints on the genesis of base-metal ores in southern and Central Sardinia. Eur. J. Mineral. 1 (5), 657–666.
Manhes, G., Minster, J.F., Allegre, C.J., 1978. Comparative uranium-thorium-lead and rubidium-strontium study of the Saint Séverin amphoterite: consequences for early solar system chronology. Earth Planet. Sci. Lett. 39 (1), 14–24.
Monna, F., Hamer, K., Lévêque, J., Sauer, M., 2000. Pb isotopes as a reliable marker of early mining and smelting in the Northern Harz province (Lower Saxony, Germany). J. Geochem. Explor. 68, 201–210.
Monna, F., Poujol, M., Losno, R., Dominik, J., Annegarn, H., Coetzee, H., 2006. Origin of atmospheric lead in Johannesburg, South Africa. Atmos. Environ. 40, 34.
Moreno, T., Alastuey, A., Querol, X., Font, O., Gibbons, W., 2007. The identification of metallic elements in airborne particulate matter derived from fossil fuels at Puertollano, Spain. Int. J. Coal Geol. 71 (2–3), 122–128.
Nory, R.M., Figueiredo, A.M.G., Souto-Oliveira, C.E., Babinski, M., 2021. Urban contamination sources in tunnel dusts from São Paulo city: elemental and isotopic characterization. Atmos. Environ. 254, 118188.
Oliveira, C., Pio, C., Caseiro, A., Santos, P., Nunes, T., Mao, H., Luahana, L., Sokhi, R., 2010. Road traffic impact on urban atmospheric aerosol loading at Oporto, Portugal. Atmos. Environ. 44 (26), 3147–3158.
Ostic, R.G., Russell, R.D., Stanton, R.L., 1967. Additional measurementsof the isotopiccompositionof lead from stratiform deposits. Can. J. Earth Sci. 4, 245–269.
Plasencia Sánchez, E., Sánchez-Soberón, F., Rovira, J., Sierra, J., Schuhmacher, M., Soler, A., Torrentó, C., Rosell, M., 2023. Integrating dual C and N isotopic approach to elemental and mathematical solutions for improving the PM source apportionment in complex urban and industrial cities: case of Tarragona – Spain. Atmos. Environ. 293, 119449.
Rahn, K.A., Silicon and aluminum in atmospheric aerosols: crust-air fractionation?. Atmos. Environ. 1967 10 8 597–601, 1976.
Querol, X., Alastuey, A., Pey, J., Cusack, M., Pérez, N., Mihalopoulos, N., Theodosi, C., Gerasopoulos, E., Kubilay, N., Koçak, M., 2009. Variability in regional background aerosols within the Mediterranean. Atmospheric Chemistry and Physics 9 (14), 4575–4591.
Ray, I., Das, R., 2023. A lingering legacy of leaded gasoline in Southeast Asia. Commun. Earth Environ. 4 1, 468.
Ray, I., Misra, S., Chen, M., Wang, X., Das, R., 2024. Entrapment of atmospheric particle bound heavy metals by ferns as evidenced by lead (Pb) isotope and MixSIAR: Implications for improving air quality. J. Hazard. Mater. 134014.
Rovira, J., Sierra, J., Nadal, M., Schuhmacher, M., Domingo, J.L., 2018. Main components of PM10 in an area influenced by a cement plant in Catalonia, Spain: seasonal and daily variations. Environ. Res. 165, 201–209.
Rovira, J., González, N., Nadal, M., Domingo, J.L., Schuhmacher, M., 2024. Air concentrations of trace elements in a municipality under the influence of Tarragona petrochemical complex: human health risks. Environ. Res. 117859.
Sánchez-Soberón, F., Rovira, J., Sierra, J., Mari, M., Domingo, J.D., Schuhmacher, M., 2019. Seasonal characterization and dosimetry-assisted risk assessment of indoor particulate matter (PM10-2.5, PM2.5-0.25, and PM0.25) collected in different schools. Environ. Res. 175, 287–296.
Sangster, D.F., Outridge, P.M., Davis, W.J., 2000. Stable lead isotope characteristics of lead ore deposits of environmental significance. Environ. Rev. 8 (2), 115–147.
Settle, D.M., Patterson, C.C., 1980. Lead in albacore: guide to lead pollution in Americans. Science 207 (4436), 1167–1176.
Shepard, D., 1968. A two-dimensional interpolation function for irregularly-spaced data. In: Proceedings of the 1968 ACM National Conference, New York, 27-29 August 1968, pp. 517–524. https://doi.org/10.1145/800186.810616.
Stock, B.C., Semmens, B.X., 2016. MixSIAR GUI User Manual - Version 3.1. Available from: http://github.com (Accessed 10 January 2024).
Sun, Y., Hu, X., Wu, J., Lian, H., Chen, Y., 2014. Fractionation and health risks of atmospheric particle-bound as and heavy metals in summer and winter. Sci. Total Environ. 493, 487–494.
Tatsumoto, M., 1973. Time differences in the formation of meteorites as determined from the ratio of lead-207 to lead-206. Science 180, 128–1279.
US-EPA — United States Environmental Protection Agency, 1989. Risk Assessment Guidance for Superfund Volume I Human Health Evaluation Manual (Part A). EPA/540/1–89/002. https://www.epa.gov/risk/risk-assessment-guidance-superfund-rags-part.
US-EPA — United States Environmental Protection Agency, 2009. Risk Assessment Guidance for Superfund (RAGS), Volume I Human Health Evaluation Manual (Part F, Supplemental Guidance for Inhalation Risk Assessment). EPA-540-R-070-002 OSWER 9285, pp. 7–82. https://www.epa.gov/risk/risk-assessment-guidance-superfund-rags-part-f.
Véron, A., Flament, P., Bertho, M.L., Alleman, L., Flegal, R., Hamelin, B., 1999. Isotopic evidence of pollutant lead sources in Northwestern France. Atmos. Environ. 33, 3377–3388.
Widory, D., Fiani, E., Le Moullec, Y., Gruson, S., Gayrard, O., 2004. Développement d'une méthode de caractérisation des contributions des sources fixes aux émissions atmosphériques de particules utilisant le traçage multi-isotopique. In: Application au cas de l'agglomération parisienne. (Doctoral dissertation in French), p. 115, 54 figures, 19 tableaux. BRGM/RP-53335-FR.

Widory, D., Liu, X., Dong, S., 2010. Isotopes as tracers of sources of lead and strontium in aerosols (TSP & PM2. 5) in Beijing. Atmos. Environ. 44 (30), 3679–3687.
Woodhead, J., 2002. A simple method for obtaining highly accurate Pb isotope data by MC-ICP-MS. J. Anal. At. Spectrom. 17 (10), 1381–1385.
Wu, P.C., Huang, K.F., 2021. Tracing local sources and long-range transport of PM_{10} in Central Taiwan by using chemical characteristics and Pb isotope ratios. Sci. Rep. 11 (1), 7593.
Zartman, R.E., Doe, B.R., 1981. Plumbotectonics—the model. Tectonophysics 75 (1–2), 135–162.